ISSN: 3169-3844
Volume 7, Number 4, 2021
Journal of Physical Sciences and Engineering

FEM SIMULATION OF TEMPERATURE DISTRIBUTION IN THE GROWTH OF SILICON CARBIDE CRYSTALS BY SUBLIMATION GROWTH METHOD

Clement Ogbonda
Department of Physics, Ignatius Ajuru University of Education
Rumuolumeni, Port Harcourt, Rivers State, Nigeria

ABSTRACT

Finite element method simulation of temperature distribution during sublimation growth of SiC single crystals by sublimation method. We consider the evolution of temperatures at the SiC source and at the SiC seed crystal, which are highly relevant to the quality of the grown crystals, but inaccessible to direct measurements. The simulations are based on a transient mathematical model for the heat transport, including heat conduction, radiation, and induction heating. Varying the position of the induction coil as well as the heating power, it is shown that the measurable temperature distribution between the bottom and the top of the growth apparatus can usually not be used as a simple indicator for the respective temperature distribution between SiC source and seed. Moreover, it is shown that the one dimensional symmetry is easily broken by the geometry or the temperature distribution. it is observed that SiC seed is unstable because variations in the geometry may give rise to a positive feedback in the growth and etch rates .

Key words: silicon carbide, seed, finite element method, sublimation method, temperature distribution

INTRODUCTION

Crystalline materials are essential for modern electrical engineering. Apart from silicon there are other crystalline semiconductors that are very attractive for certain applications. One of these is silicon carbide (SiC). It representative wide-bandgap semiconductor material It has many remarkable properties which make it a very promising semiconductor material (Ogbonda 2020). Due to its characteristics of low consumption, high efficiency and high power, SiC is expected to revolutionize the power electronics industry. Some of the potential applications of silicon carbide are in high-temperature, -frequency, and -power electronic devices (Shengtao et al 2022). Others make use of the wide bandgap: UV radiation detectors and even blue-light lasers. Light emitting diodes (LEDs) have already been in commercial production for some years. Also some other electronic devices may become commercial in the near future. The large-scale manufacturing of electronic devices requires a continuous production of good-quality wafers. In silicon carbide growth there are still some basic problems to be resolved that limit the commercial utilization of the material (Raback 1999). These problems are related to crystal size and both macroscopic and microscopic defects. The process involves sublimation of a heated SiC powder charge in the bottom region of a graphite crucible, transport of sublimated vapor through an inert gas environment, and condensation on a cold pre-oriented seed mounted at the bottom of the lid of the crucible.

Several studies have been conducted to study the growth phenomena, particularly through post-growth analysis of grown crystals and thermal modeling of the growth system. However, very little is known of the effect of various process parameters on the rate of SiC growth. On the other hand, the growth kinetics of semiconductor PVD (and CVD) processes has been studied in detail (Tuominen et al 1996),(Müller et al 1997), (Glass et al 1997),(Allan 1997.). For example, Bloem and Giling (2018) formulated some simple growth kinetics for the semiconductor CVD processes. Kaneko (2017), Glass et al (1997) compiled several growth models for various kinds of PVD (and CVD) processes. He considered the impinging molecular flux of a rate-determining species in equilibrium, and used a sticking coefficient to relate the growth rate with equilibrium vapor pressure of the species. As one of the most important third-generation semiconductor materials, SiC has received

widespread attention due to its wide band gap, high breakdown field strength, high thermal conductivity, and high carrier saturation mobility (Raback et al 1997, Raback et al 1998, Raback et al 1999). Devices based on SiC substrate have been widely used in important fields such as electrical vehicles and 5G communication (Kordina 1994, Bechstedt et al 1997). Physical vapor transport (PVT) is the main method for growing a large-size SiC single crystal, which needs to be cost-effective and defect-free. SiC powder is used as the source material during the PVT growth of a SiC single crystal (Tuominen et al 1997).

Wang et al.(2021), found that the sublimation of SiC powder was insufficient, and they increased the crystal growth rate by the optimization of powder packaging .

Lebedev, (2019) studied the sublimation process of SiC powder in a traditional structure by the finite element method and found that the sublimation rate of SiC powder can be improved by adjusting the coil height (Geiser,et al 2006). However, there are few research works on the relationship between the graphite structure design and the utilization rate of SiC powder (Liu, et al 2010). This involves equations of change that describe how mass, energy and electric currents are transported in the growth apparatus. These are partial differential equations that are solved with the finite element method, FEM..

The seeded sublimation growth process has been modeled for almost as long as the method has been known. The modeling of sublimation growth has by no means been in the cutting edge in applying the newest methods. The methods have usually been first developed in other fields and only later applied to the problem of sublimation growth. Most of the simulation papers related to the simulation of sublimation growth are therefore quite sparse in computational details.

The sublimation growth process is driven by super saturation due to the temperature difference between the source and the seed. This driving force may be estimated by equilibrium thermodynamics. It is the more relevant the closer the system is to equilibrium. Sublimation growth of SiC is close to equilibrium conditions due to the high temperatures and slow mass transport rates. Equilibrium calculations may also be used to identify the most important chemical species in the system. The equilibrium chemistry related to SiC growth has been analyzed in several papers (Pons, et al (1996), Lilov, et al (1979), Lilov (1989). In most papers only the three most important species (Si, Si2C, SiC2) have been considered. Reactive process gases quickly increase the number of important species (Lilov et al 2017), (Lilov et al 2016), Allendorf (1993). The equilibrium calculations can unfortunately only give trends, *i.e.*, tell whether the growth is possible or not, but it does not tell anything about the growth rate. The lack of accurate kinetic data at high temperatures has been the bottleneck in applying kinetic calculations to the sublimation growth process. Such treatise have been written for the CVD growth, see for example References , (Allendorf and Kee. 2020),

This study is aimed at examining the Temperature Distribution in the growth of Silicon Carbide Crystals by Sublimation growth method.

Nomenclature

h	local heat generation in unit volume
$\overrightarrow{e_n}$	normal of the surface,
q	heat flux
h_T	heat transfer coefficient, and
T_{ext}	external temperature.
$G(\overrightarrow{r}\hat{}\vec{r})$	*Gebhart factor*
F	*view factor* between two points
β and $\beta\hat{}$	sharp angles formed by the surface normals
Ω	axisymmetric volume
$\partial\Omega$	axisymmetric volume with boundary
U	Test function space
φ_I	basis functions

t_i	Unknown temperatures at selected points and
I	The number of nodes.
q	global basis functions by
Ai	Area of an surface element
Gji	Discrete Gebhart factor and
Is	Number of surface elements

Growth from Melt

Most commercially utilized single crystal semiconductor boules are grown from a melt or solution, but this is not a feasible option for SiC growth. SiC does not have any liquid phase in normal engineering conditions. Calculations have indicated that stoichiometric melting is possible only under pressures exceeding 105 bar at temperatures higher than 3200^{O}C. Even if the solubility of carbon in silicon melt ranges from 0.01% to 19% in the temperature interval from 1412 to 2830^{O}C, at high temperatures the evaporation of silicon makes the growth unstable. The solubility of carbon can be increased by adding certain metals to the melt (*e.g.*, praseodymium, terbium, scandium). This would, in principle, enable the use of crystal pulling techniques, such as *Czochralski growth*. Unfortunately there is no crucible material available that would be stable with these melts. It is also speculated that the solubility of the added metals in the growing crystal is too high to be acceptable in semiconductor materials (Glass et al 1997, Yoder and Davis. 1989). In spite of all the problems, SiC was grown from melt at 2200^{O}C and 150 bar in a recent study. The crucible was made of graphite and it also acted as the carbon source. A 1.4-inch crystal was demonstrated (Hofmann, et al 1998). The seeded sublimation growth, also known as *physical vapor transport* (PVT), is the method of the present study. It is historically referred to as the modified Lely method. The geometry was initially quite similar to the Lely geometries but the difference is the use of a seed crystal which results in a more controlled nucleation. The seeded sublimation process is nowadays the standard method for growing bulk monocrystalline silicon carbide (Tairov and Tsvetkov 1981,. Glass et al 1997, Tairov 1995, Augustine, et al 1998, Chourou, et al 1998). In the process polycrystalline SiC at the source sublimes at a high temperature, ($1800 - 2600$ ^{0}C) and low pressure. The resulting gases travel through natural transport mechanisms to the cooler seed crystal where crystallization due to supersaturation takes place. The seed crystal is usually situated at the top of the crucible in order to prevent contamination by falling particles. There are different flavors of sublimation growth. The most important factor that can be varied, is the crucible design and the temperature distribution related to it. The crystals tend to grow along isotherms and therefore the shape of the temperature distribution must be carefully designed. The most common design is to put the source at the bottom of the crucible so that the surface of the source is facing the growing surface. This minimizes the source-to-seed distance

PHYSICAL MODELS

The temperature distribution of the crucible is solved from the energy equation. At the high temperatures radiation dominates the energy transport and convection may be neglected. The system changes gradually with time due to the crystal growth. The changes are, however, so slow that the system is assumed to be in a thermally stable state, and the energy equation becomes stationary.

$$-\nabla.(k.\nabla T) = h. \qquad 1.$$

The energy equation may have fixed (Dirichlet) or flux (Neumann) boundary conditions. Often the flux boundary conditions written as

$$-\nabla.(k.\nabla T).\overrightarrow{e_n} = q(\vec{r},T), = h_T(\vec{r},T)(T - T_{ext}) \qquad 2.$$

In particular, heat transfer by radiation is of the form

$q(\vec{r},T) = \epsilon\sigma_{SB}(T^2 + T_{ext}^2)(T + T_{ext})$ 3.

A special case of radiation is a boundary condition for a surface that sees itself at least partially. This makes the local external temperature dependent on the temperature of the boundary itself. Therefore the external temperature is calculated from the following equation,

$$T_{ext}^4(\overrightarrow{r}) = \frac{1}{\epsilon(r^2)}\int \epsilon(\vec{r})G(\overrightarrow{r^{\wedge}},\vec{r})T^4(\overrightarrow{r^{\wedge}})\ dS_{\overrightarrow{r^{\wedge}}} \quad 4$$

The Gebhart factors are solutions of the integral equation

$$G\left(\overrightarrow{r^{\wedge}},\vec{r}\right) - \int F\ \left(\overrightarrow{r^{\wedge}}\vec{r}\right)(1-\in\left(\overrightarrow{r^{\wedge}}\right)G\left(\overrightarrow{r^{\wedge}},\vec{r}\right)dS_{\overrightarrow{r^{\wedge}}} = F(\overrightarrow{r^{\wedge}},\vec{r}) \in (\vec{r}), \quad 5.$$

view factor depends only on the geometry of the system and is defined as

$$F(\vec{r},\vec{r}) = \frac{cos\beta\left(\vec{r},\overrightarrow{r^{\wedge}}\right)cos\beta^{\wedge}(\overrightarrow{r^{\wedge}},\vec{r})}{\pi\left|\vec{r}-\overrightarrow{r^{\wedge}}\right|^2}\chi(\vec{r},\overrightarrow{r^{\wedge}}) \quad 6$$

where β and $\beta^{\wedge}$are the sharp angles formed by the surface normals and the line connecting the points points $\vec{r}$ and $\overrightarrow{r^{\wedge}}$. Function χ is one if the points $\vec{r}$ and $\overrightarrow{r^{\wedge}}$. see each other and zero if there is an obstacle between the points (Atherton, et al 1993, Bor nside et al 1990). When a system is built of several parts the thermal contact is seldom perfect. This creates difficulties since the gaps between the different parts are usually too small to be taken into account in creating the computational geometry. A way to tackle this problem is to allow the temperature to be discontinuous over the gaps. The boundary conditions must be set on both sides of the gap. For linear heat transfer the boundary condition at the sides are expressed by a dual boundary condition

$$\begin{cases} q(\vec{r},T) = h_T(\vec{r},T)(T - T^{\wedge}) \\ q^{\wedge}(\vec{r},T) - h_T(\vec{r},T)(T^{\wedge} - T) \end{cases} \quad 7.$$

For radiation, it is not necessary to calculate the view factors since it is obvious that at the interface the walls see the other side of the gap in a full angle. The heat transfer coefficient may now be analytically calculated to be

$$h_T = \frac{\epsilon\epsilon^{\wedge}}{\epsilon+\epsilon^{\wedge}-\epsilon\epsilon^{\wedge}}\sigma_{SB}\left(T + T^{\wedge}\right)(T^2 + T^{\wedge 2}) \quad 8.$$

NUMERICAL ANALYSIS

The finite element method is used to solve the energy equation. This equation will be considered first since the finite element method is most conveniently introduced for this case. The discretization of the differential equation starts with writing the corresponding variational formulation, a so-called *weak form* of the equation. In the axisymmetric case equation yields

$$-\frac{\partial}{\partial z}\left(k_z\frac{\partial T}{\partial z}\right) - \frac{1}{r}\frac{\partial}{\partial r}\left(k_r T\frac{\partial T}{\partial r}\right) = h \quad 9$$

The thermal conductivity tensor is assumed to be diagonal. Integrating over an axisymmetric volume Ω with boundary $\partial\Omega$ and applying Green'stheorem, Equations (9) and (2) give

$$\int_\Omega \left(k_z\frac{\partial v}{\partial z}\frac{\partial T}{\partial z} + k_r T\frac{\partial T}{\partial r}\frac{\partial v}{\partial r}\right) r\ dr\ dz + \int_{\partial\Omega} rvqdl\ = \int_\Omega\ vhrdrdz \quad \forall v \in U \quad 10$$

The unknown temperature distribution is expressed as a linear combination of the basis functions φ_I

$$T(\vec{r}) = \sum_{i=1}^{1} t_i \varphi_i \vec{r} \qquad 11$$

The real-life geometries are seldom rectangular. Therefore also the elements used for discretization should be nonrectangular. In the axisymmetric case the global coordinates *r* and *z* are expressed with the help of normalized coordinates $\xi \in [-1,1]$. and $\eta \in [-1,1]$ The mapping

$$r(\xi,\eta) = \sum_{i=1}^{4} f_i(\xi,\eta)\ r_i \qquad 12$$

$$z(\xi,\eta) = \sum_{i=1}^{4} f_i(\xi,\eta)\ z_i \qquad 13$$

transforming the local point to the global coordinate system. The bilinear isoparametric element is defined by the following basis functions

$$f_i(\xi,\eta) = \frac{1}{4}(1-\xi)(1-\eta)$$

$$f_2(\xi,\eta) = \tfrac{1}{4}(1+\xi)(1-\eta) \qquad (14)$$

$$f_3(\xi,\eta) = \frac{1}{4}(1+\xi)(1+\eta)$$

$$f_4(\xi,\eta) = \frac{1}{4}(1-\xi)(1+\eta)$$

The basis functions above are local basis functions associated with a given element. They are related to the global basis functions by q

$$\varphi_i \vec{r} = \begin{cases} f_j(\xi,\eta) \\ 0 \end{cases}$$

if $\vec{r}$ is within an element whose local node *j* is the global node *i;* *;* otherwise*: Unknown temperature*

$$\sum_{i=1}^{1}[\int(k_r \frac{\partial\varphi_j}{\partial z}\frac{\partial\varphi_i}{\partial z} + k_z \frac{\partial\varphi_j}{\partial r}\frac{@ri}{\partial r})rdrdz]t_i + \int \varphi_j q(\vec{r}, t_1 t_2 \dots tN)rdl = \int \varphi_j hrdrdz, j = 1, \dots I \qquad (15)$$

The integration is performed numerically using Gaussian quadratures. The procedure results in a matrix equation that may be solved applying standard methods of linear algebra. The type of heat exchange *q* determines the nature of equation (15). If it is linear with temperature also the total equation is at least pseudo-linear. There might still be temperature dependent parameters, such as the thermal conductivity. If the heat exchange is due to radiation, the equation can still be solved as if it were linear. This requires the use of Equation (3). Linear boundary conditions can be split into two,

$$\int_{\partial\Omega} \varphi_j q_i rdl = \sum_{i=1}^{1}\left(\int_{\partial\Omega} \varphi_i \varphi_j h_T rdrdz\right) t_i - \int_{\partial\Omega} \varphi_j h_T T_{ext} rdrdz \qquad 17$$

Here, the first term is linear with respect to *T* and the second term is constant, or can at least be handled as constant. Truly nonlinear boundary conditions may lead to problems in convergence

when treated as linear. This is the case for a boundary that is coupled to itself through the Gebhart factors. The discrete counterpart of Equation (2) is

$$q_1 = \sigma s B \epsilon_i \left(T_i^4 - T_{ext,i}^4\right) \quad 18$$

$$T_{ext,i}^4 = \frac{1}{A_i \epsilon_i} \sum_{k=1}^{1} \epsilon_k \, A_k G_{ki} T_k^4 \quad 19.$$

Gji are solutions of

$$G_{ji} - \sum_{k=1}^{1} F_{jk}(1 - \epsilon_k) G_{ki} = F_{ji} \, \epsilon_i \quad 20.$$

Fij the view factor between two surface elements,

$$F_{ij} = \frac{1}{A_i} \int \int \frac{cos\beta_i(\vec{r_i},\vec{r_j}) cos\beta_j(\vec{r_i},\vec{r_j})}{\pi \left|\vec{r_i} - \vec{r_j}\right|^2} \chi\left(\vec{r_i}\vec{r_j}\right) ds_i ds_j \quad 21.$$

The difference between linear and nonlinear models is important in selecting the best method for solving the equations. We have basically two choices how to solve the nonlinear equation. The simple one is to linearize radiation according to the formula (3). If, however, radiation is the dominating heat-transfer mechanism this may lead to very poor convergence. In this case Newton-Raphson type of iteration can be used. In the linearized method the external temperature is calculated from the previous iteration step (explicit method), whereas in Newton- Raphson iteration it is also regarded as an unknown (implicit method). If the contribution of radiation is treated simply as a source term it results in severe convergence problems for well-isolated systems even though for most systems it works perfectly well.

Linear Iteration

In the linear iteration the solution satisfies the equation

$$A(t)t = f(t), \quad 22.$$

Where

$$A_{ji} = \int_\Omega \left(k_z \frac{\partial \varphi_j}{\partial z} \frac{\partial \varphi_i}{\partial z} + k_r \frac{\partial \varphi_j}{\partial r} \frac{\partial \varphi_i}{\partial r}\right) r dr dz + \int_{\partial\Omega} \varphi_j \varphi_i h_T r dl \quad 23$$

and

$$f_j = \int_\Omega \varphi_j h r dr dz + \int_{\partial\Omega} \varphi_j h_T T_{ext} r dl \quad 24$$

The iteration scheme is

$$t^{(m+1)} = A^{-1}\left(t^{(m)}\right) f\left(t^{(m)}\right) \quad 25$$

Newton-Raphson Iteration

In the Newton-Raphson iteration we must find vector t that satisfies the nonlinear equation

$$g(t) = A(t)t + b(t) - f = 0$$

Where

$$A_{ji} = \int_\Omega \left(\left(k_z \frac{\partial \varphi_j}{\partial z} \frac{\partial \varphi_i}{\partial z} + k_r \frac{\partial \varphi_j}{\partial r} \frac{\partial \varphi_i}{\partial r}\right) r \, dr \, dz\right) \quad 26.$$

$$b_j = \int_{\partial\Omega} \varphi_j \sigma_{SB} \epsilon_i \left(t_1^4 - \frac{1}{A_i \epsilon_i} \sum_{k=1}^{1} \epsilon_k \, A_k G_{ki} t_k^4\right) r \, dl \, dz \quad 27$$

$$f_j = \int_\Omega \varphi_j h r dr dz \quad 28$$

The iteration scheme is

$$t^{(m+1)} = t^{(m)} - J^{-1}\left(t^{(m)}\right)g(t^{(m)}) \qquad 29$$

And

$$\frac{\partial b_j}{\partial t_i} = \int_{\partial\Omega} 4\varphi_j \sigma s B \epsilon_i (t_i^3 - \frac{A_j \epsilon_j}{A_i \epsilon_i} G_{ji} t_j^3) r dl \qquad 30$$

The implicit Newton-Raphson type of iteration may lead to a very different type of matrix equation compared to the linear iteration. The elements within a closure that see each other form a full block in the matrix, while linear iteration leads to a sparse matrix with a banded structure.

The solution of the energy equation was verified in quite a complicated geometry arising from Czochralski growth of silicon crystals. The comparison was done against the commercial FIDAP code (Savolainen 1996) and against another in house code (Järvinen, 1996). Also a sublimation type of geometry was verified against results by two international research groups (Communication with Jean-Marc 1998). Both cases showed accurate results with a very good convergence. It was also checked that the power input was closely the same as the heat transfer through the external boundaries. From the mathematical point of view the most interesting feature of the energy equation is the nonlinearity. It may be caused by variable thermal conductivity or by radiation. The temperature dependence of thermal conductivity caused no convergence problems whatsoever, and neither did the linearized radiation to external temperature. However, radiation within a closure is a more critical problem. The Newton-Raphson iteration proved to be quite necessary particularly for well-isolated systems. Therefore a special test case was set up to investigate this phenomenon. It helps in deciding when the computationally more expensive Newton-Raphson iteration should be used. The test case consists of an axisymmetric closure surrounded by an insulation. The inner diameter and inner height are both 10 cm, as well as the thickness of the insulation. No heat source is included. At all the surfaces diffuse gray radiation with unity emissivity is assumed. The ambient temperature is set to be quite high, 3000 K, while the initial guess is a constant temperature distribution of 1000 K. This provides with a good test case since it is easily concluded that the correct solution of this problem is a constant temperature distribution of 3000
K. The computational mesh used in the calculations is shown in Figure 1.

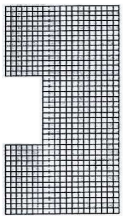

Figure 1: ***Computational mesh with 709 elements and 777 nodes***

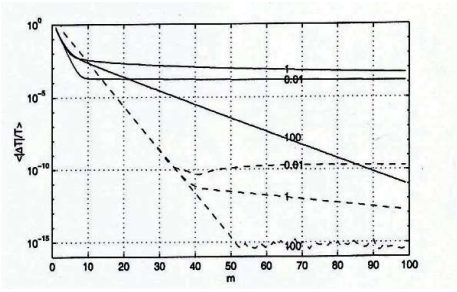

Figure 2**:** ***Mean relative change as a function of iteration step for linear (solid line) and Newton-Raphson iteration (dashed line) with different values of thermal conductivity (0.01, 1.0 and 100 W/mK).***

The thermal conductivity of the insulation was varied in order to investigate how it affects the rate of convergence of the two different models. The values used for the thermal conductivity, 0.01, 1.0

and 100.0 W/mK, cover all typical materials. The mean relative change as a function of iteration step is presented in Figure 2. As may be seen the error of the Newton-Raphson iteration decreases rapidly and settles then down to a value that characterizes the maximum numerical accuracy of the solution.

The speed of convergence does not depend on the thermal conductivity Accuracy with five digits is obtained in about ten iterations. The situation is quite different for the linear iteration. Now the speed of convergence depends very much on the thermal conductivity. When thermal conductivity is small the error seems to be small but it is just a sign that the equation is so stiff that the solution hardly changes. This is illustrated in Figure 3 that shows the minimum temperature as a function of iteration step. For well-isolated systems the system converges extremely slowly and therefore linear iteration fails desperately. Therefore the use Newton-Raphson iteration which seems to be superior to the linearized approach.

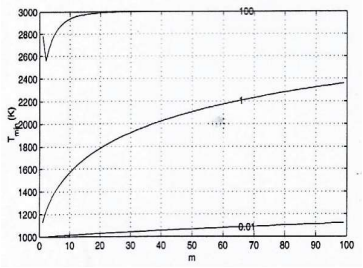

Figure 3: ***Minimum temperature in the linear iteration as a function of iteration step with different values of thermal conductivity (0.01, 1.0 and 100 W/mK).***

RESULTS AND DISCUSSION

So far the sublimation growth of SiC may seem to be quite simple. It involves only the problem of placing a hot source to face a slightly colder seed within a closed cavity. The growth is controlled by the temperature gradient and by the choice of the carrier gas and its pressure. Unfortunately, there are some intrinsic problems that complicate the design and building of growth furnaces. These problems may be efficiently studied by the use of simulations. Let us look at a typical sublimation growth geometry presented in Figure 4. A crucible made of dense graphite forms a semi closed cavity. At the top of the cavity there is a SiC seed and at the bottom of the cavity there is a SiC source. The crucible is surrounded by insulation made of porous graphite. For temperature measurement two openings are provided for pyrometers that determine the temperature by the radiation emitted from the crucible surface. The whole system is surrounded by an induction coil that may be moved in the axial direction. The inner diameter of the crucible is 5.0 cm and the outer diameter of the insulation is 15.0 cm. At the top of the crucible the thickness of the insulation is 3.0 cm and at the bottom 10.0 cm, correspondingly. The coil is 10.0 cm in length, 16.0 cm in diameter and its center is aligned with the inner bottom of the crucible.

Table 1: ***Material parameters used in the example simulations.***

Material	ϵ	$k(W/mk)$	$\sigma(1/\Omega m)$
Source	0.8	1.0	100.0
Seed	0.8	$451700T^{-1.29}$	10000.0
Crucible	0.9	$125868/(T+615.9)$	$6.67E4/1(+\frac{T}{2500})$
Insulation	0.9	$2.146E-9T^2-1.43E-5T+0.367$	$245.7/(1+T/2500)$

The material parameters used in the example calculations are presented in Table 1. They are typical, yet not necessarily accurate values for the various parameters. The properties of silicon carbide source and seed are discussed in papers (Kitanin et al 1998).

In solving the induction heating problem it was assumed that the vector potential vanishes at infinity which in this case meant a moderate distance of 30 cm. An additional increase in this distance did not affect the results significantly. In the energy equation the temperature was assumed to be fixed to room temperature at the bottom of the insulation, and on other directions black body radiation to room temperature was assumed. Inside the crucible the heat transfer included conduction in the gas phase and radiation between the crucible walls. Also the heat transfer in the pyrometer holes was modeled assuming wall-to-wall radiation.
In solving the vector potential around 10000 bilinear elements were used and for the temperature around 6000 elements. The iteration converged without any problems. Around 20 iterations for the temperature and 3 iterations for the vector potential were required when the termination criteria was a relative error of 10^{-5}. The overall computational time on a powerful workstation was a couple of minutes. Figure 5, shows typical results from the vector potential calculations.

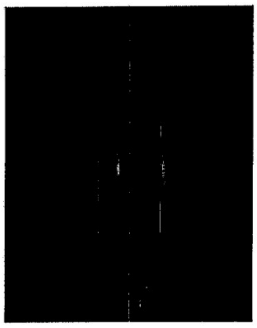

FIgure 4: Components of the vector potential. In-phase component on the right and out-of-phase component on the left.

In the picture the components of the vector potential have been normalized so that their maximum values are equal. In reality the out-of-phase component is significantly smaller in magnitude. The vector potential is mapped to the scope used in thermal calculations as shown in Figure 5.

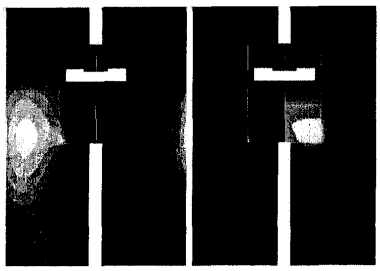

Figure 5: a) Components of the vector potential mapped to the scope used in the thermal simulations. b) Heat generation L´ induction on the left and the resulting temperature distribution on the right.

The vector potential is then used to calculate the local heat generation due to Ohmic losses. The losses are concentrated on the crucible walls. In the thermal calculations the heat generation is normalized so that the total heating power agrees with the desired value. The picture shows also the resulting temperature distribution. The temperature distribution may be slightly affected by altering the parameters of the induction heating. In the simulation of figure 7 the frequency was increased from 50 kHz to 200 kHz and the coil was lowered to 1.5cm. As a result the heating is concentrated more clearly on the surface and on the crucible corner. Ideally we would like to heat also the inner parts of the crucible and therefore lower frequencies are generally favored. They also couple in a lesser extent to the porous graphite used for thermal isolation. Figures such as 4, 5 and

6 may give insight in the governing phenomena but they do not provide the quantitative information requiredin thermal design.

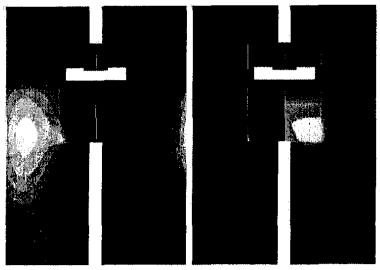

Figure 6: a) Components of the vector potential with increased frequency and lower coil position. b) Heat generation by induction and the temperature distribution.

Figure 7 shows temperature at given points as a function of heating power. As might be expected the temperatures increase monotonically with heating power. The system is set up so that heating is strongest under the source. The energy must escape somewhere and the natural way is through the weakest isolation which results to a heat flux from bottom to top.

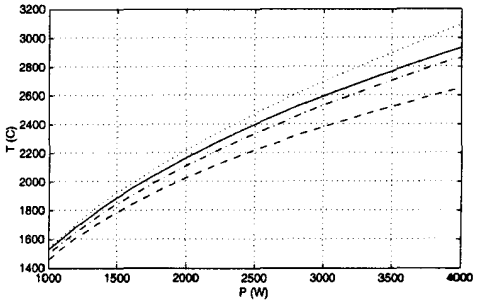

Figure 7: Temperatures at lower pyrometer hole (solid line), uplwrpyrometer hole (dashed line), source bottom (dotted line), source surface (dash-dot line) as a function of line) of heating power

Heat flux is directly related to temperature and therefore the source is hotter than the seed. Unfortunately the source material is typically porous SiC powder that has a very poor thermal conductivity. Theoretical calculations have shown that the conductivity of ideal porous SiC is less than 1 W/mK , (Kitanin et al 2019) . This means that it is difficult to apply a large heat flux through the source and that it will automatically result to large temperature differences within the source. The thicker the source the more prominent this problem is. Closely the same heat flux is also transferred from the surface of the source to the seed. Now the temperature difference is much smaller since radiation transports energy very efficiently at high temperatures. The temperature difference between the source and the seed is presented in Figure 8. The same picture also shows the temperature difference with a reduced amount of powder. The heat flux is now larger and therefore the temperature difference between the source and the seed is also larger.

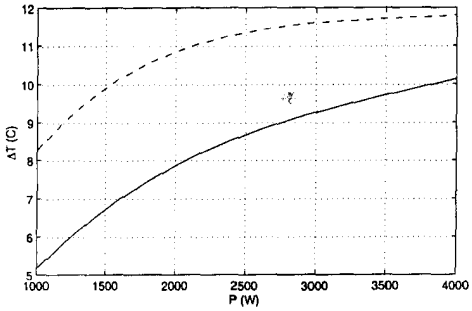

Figure 8: Temperature difference between the source and the seed as a of heating power with 20 mm (solid line) and 10 mm (dashed line) of source powder.

5.1 **Feedback for Temperature Control**

When the input power is known the calculated temperatures may be compared to experimental results. Unfortunately, there are some internal losses in the induction heating system and also the thermal conductivities at high temperatures are badly known. When we want to know the temperatures inside the crucible as accurately as possible we use the measured temperatures to calibrate the simulation. This is done by using a feedback loop to set the heating power so that the temperature estimated by the simulations agrees with the value measured by the pyrometer. A similar feedback is also used in the practical experiments in order to keep the system at a fixed temperature during the growth process.

Figure 9, shows the temperature at the axis and wall temperature projections at different coil positions, $-30, +10, +10\ and\ +30mm$. The zero position is aligned with the bottom of the crucible cavity.

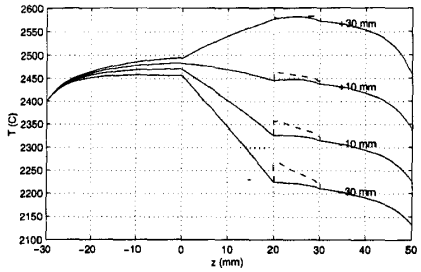

Figure 9: Temperature at the axis and inner crucible walls (dashed line) for coil positions —30, — 10, +10 and ÷30 mm when the temperature measured by the lower pyrometer is kept constant.

By moving the coil it is possible to influence the temperature gradient. It is important that the sign of the temperature gradient can be changed by coil movement because the quality of the crystal may benefit if the seed is etched in the start of the process (Anikin, and Madar 1997). The temperature measured by the lower pyrometer may be quite different from the temperature of the seed. Feedback using the upper pyrometer for temperature control might be more useful as is seen in Figure 10.

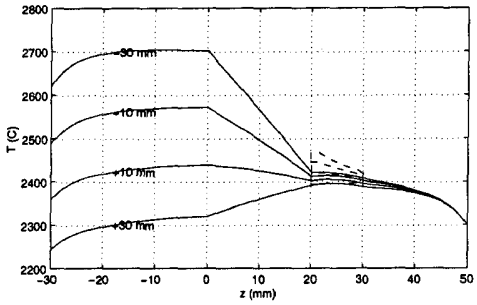

Figure 10: Temperature at the axis and inner crucible walls (dashed line) for different coil positions with a solid SIC source.

The temperature of the seed correlates now much better with the temperature used for feedback. The holes used for temperature control create a cold finger in the temperature distribution. This may result in a convex growth front which may be desired particularly if seed enlargement is required. The pyrometer holes should therefore be carefully designed for optimal crystal-growth shape. The Figures 6 and 7 also reveal a problem that is an intrinsic property of the simple geometry under discussion. The temperature gradient on the side wall is significantly larger than the temperature gradient at the axis. This is an unfortunate result of the poor thermal conductivity of the source material when compared to the walls made out of dense graphite.
This feature in the temperature distribution means that the source material is mostly consumed near the walls whereas even consumption would be favored. The problem might be solved by increasing the thermal conductivity of the source material. This might be achieved by using solid SiC source as is done in Figure 11. Now the temperature gradient at the axis and at the side wall are nearly equal and thus the source is consumed more evenly. Also the temperature difference between the source and the seed is now larger since the heat flux going through the solid source is larger than the heat flux going through the porous source.

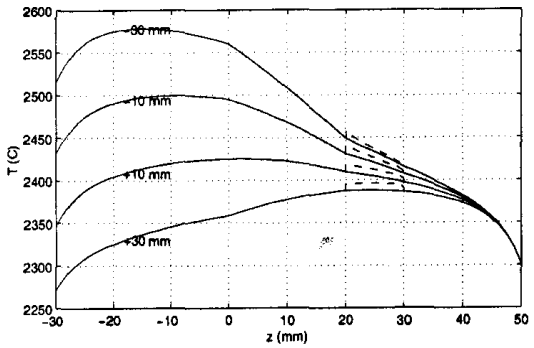

Figure 11: Temperature at the axis and inner crucible walls (dashed line) for different coil positions with a solid SIC source.

Heating the Source Evenly

Let us pay some more attention to the problem of heating the source evenly. Ideally, we would only heat up the source itself but it is difficult with the means that are available. As the RF-field couples quite poorly with the source, induction it is not a feasible method for direct heating. It seems also impossible to heat the source directly at the active surface since it should preferably face the colder seed. Therefore, the only practical heating method is to heat the source via the hot walls. Unfortunately, the thermal conduction of porous SiC is so bad that when we heat the powder up we are bound to introduce large temperature gradients over the powder. The warmest spots will always

be situated at the hot crucible walls. It is also difficult to control the temperature at the active surface. The larger the amount of powder the more difficult are the problems related to heating. The heating of the source material may be the most severe limitation of sublimation growth. Let us assume that we want to have constant temperature and heat flux over the active surface. If the source is cylindrical in shape we may heat it from the side or from the bottom. Heating from the bottom is a trivial case since constant temperature at the bottom will also result to constant temperature at the active surface. Heating from aside is a more involved matter. Consider a simple geometry heated from the side. It is presented in Figure 9, The problem is to heat a cylindrical source so that the temperature at the active surface is uniform. The heating element of length R = 25 mm is set at a distance A lower than the source surface. At the active surface we assume radiation to external temperature of 2500^0C At the heating element constant power generation is set. We should select A so that both the radial temperature gradient at the surface and the temperature difference within the source would be reasonably small. These two requirements are contradictory. Figure 11, shows the temperature at the interface with different values of $A=R$. When the value $A=R$ increases the temperature distribution at the surface becomes more settled, but the maximum temperature difference increases. This is shown in Figure 10. It seems that ratio $A=R$ close to unity might be quite optimal. The calculations suggest that if we require even temperature at the source surface, heating from the side should be avoided unless the thickness of the source is significantly larger than the radius of the source. Even then heating from aside must be performed very accurately in order to control the temperature at the active surface. This might not be possible with the technical means that are at disposal at such high temperatures. Also, maintaining constant heating during the growth process may require some active parts. On the other hand, heating from aside may eventually enable continuous growth techniques for long crystals. So far it seems that the SiC industry is pursuing crystal area at the expense of crystal length. Geometries favoring axial growth have, however, been reported for other materials, see (Råback et al 1998).

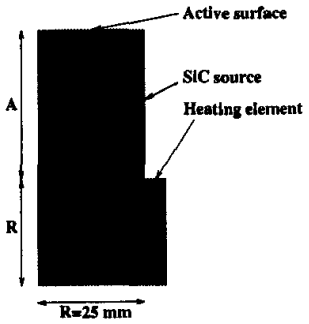

Figure 11 :Simple heating geometly when heating from aside.

CONCLUSIONS

In sublimation growth the supersaturation is ideally only due to a temperature distribution between the source and the seed. However, because the surface energy of porous SiC is slightly smaller than that of crystalline SiC the partial pressures over porous SiC are also higher than over crystalline SiC, even at the same temperature. This may lead to nucleation anywhere within the system, not only at the cold spots. In order to control the growth efficiently, the system should be set up so that the major cause for supersaturation is the temperature difference between the source and the seed. This argument together with the bad thermal conductivity of porous SiC strongly suggests that the source should rather be solid SiC . Ideally the crystal growth process would be one-dimensional. The one dimensional symmetry is easily broken by the geometry or the temperature distribution. Seed enlargement may also be required and it is achieved by carefully designed convex isotherms. In Czochralski crystal growth the shape of the growth front is easily retained because the crystal

growth is not limited by mass transport. Sublimation, on the other hand, may be unstable because variations in the geometry may give rise to a positive feedback in the growth and etch rates. Therefore, the temperature control calls for special attention in the sublimation growth process.

REFERENCES

(1) Råback, R. Nieminen, R. Yakimova, M. Tuominen, and E. Janzén. (1997) .Thermodynamic considerations on the role of hydrogen in sublimation growth of silicon carbide. *Journal of the Electrochemical Society*, 144(3):1024-1027.

(2) Råback, R. Nieminen, R. Yakimova, M. Tuominen, and E. Janzén.(2008). A coupled finite element model for the sublimation growth of SiC.*Materials Science Forum*, 264-268:65-68,

(3) Råback, R. Yakimova, M. Syväjärvi, R. Nieminen, and E. Janzén. (1999) .A practical model for estimating the growth rate in sublimation growth of SiC. *Materials Science and Engineering*, B 61-62:89-92.

(4) Bechstedt, P. Käckell, A. Zywietz, K. Karch, B. Adolph, K. Tenelsen, and J. Furthmüller.(1997) Polytypism and properties of silicon carbide. *Physica Status Solidi (b)*, 202(1):35-62.

(5) Kordina, O.(1994). *Growth and Characterisation of Silicon Carbide Power Device Material*. PhD thesis, Linköping University,

(6) Tuominen, R. Yakimova, E. Prieur, A. Ellison, T. Tuomi, A. Vehanen, and E. Janzén (1997). Growth-related structural defects in seeded sublimation-grown SiC. *Diamond and Related Materials*, 6:1272-1275.

(7) Allan.R, (1997) Crystal powers. *New Scientist*, (2086):34_37, .

(8) Yoder M. N, and R. F. Davis. (1989) Silicon carbide comes of age. *Naval Research Reviews*, (1):26-33,

(9) Tuominen.M. (1997) *Growth and Structural Characterization of Silicon Carbide Crystals*. PhD thesis, Linköping University, 1997.

(10) Chourou.K (1998) *Contribution a l'etude de la cristallogenese du carbure de silicium SiC par sublimation*. PhD thesis, Institut National Polytechnique de Grenoble,

(11). Hofmann, M. Müller, and A. Winnacker.(1998) Prospects in the use of liquid phase techniques for the growth of bulk silicon carbide crystals. In *Abstracts of the 2nd European Conference on Silicon Carbide and Related Materials*,

(12) Lilov, Yu. M. Tairov, and V. F. Tsvetkov. (1979) Study of silicon carbide epitaxial growth kinetics in the SiC system. *Journal of Crystal Growth*, 46:269-273,

(13) Pons, E. Blanquet, J. M. Deduille, I. Garcon, R. Madar, and C. Bernard.(2019) Thermodynamic heat transfer and mass transport modeling of the sublimation growth of silicon carbide crystals. *Journal of the Electrochemical Society*, 143(11):3727-3735,

(14). Lilov, Yu. M. Tairov, V. F. Tsvetkov, and B. F. Yudin.(1977) Studies of growth processes from the vapour phase of silicon carbide epitaxical layers. *Journal of Crystal Growth*, 40:59-68,

(15). Lilov, Yu. M. Tairov, V. F. Tsvetkov, and B. F. Yudin. (1976) .Studies of growth processes in silicon carbide epitaxial layers from the vapour phase. *Journal of Crystal Growth*, 32:170-178,

(16) Allendorf.M.R (2019) Equilibrium predictions of the role of organosilicon compounds in the chemical vapour deposition of silicon carbide. *Journal of the Electrochemical Society*, 140(3):747-753,

(17) Allendorf , M. D., and R. J. Kee.(2020) A model of silicon carbide vapor deposition. *Journal of the Electrochemical Society*, 138(3):841-852, .

(18) Müller, St D. Hofmann, L. Kadinski, P. Kaufmann, M. Kölbl, and E. Schmitt.(1998) Modelling of the PVT-SiC bulk growth process taking into account global heat transfer, mass transport and heat of crystallization and results on its experimental verification. *Materials ScienceForum*, 264-268:57-60.

(19) Shengtao, Z. Guofeng, F. Tie, L. and Lili Z (2022) Optimization of thermal field of 150 mm SiC crystal growth by PVT method *RSC Advances Journal 12(31): 19936–19945*

(20) Lebedev A. A. (2019) Deep Level Centers in Silicon Carbide: A Review. *Semiconductors.* 33(2):107–130.